Detecting subsurface objects and identifying voids possibilities using seismic diffractions

Julian Ivanov, Richard D. Miller, Shelby L. Peterie, and Anthony M. Hock, Kansas Geological Survey*

Summary

We used a synthetic seismic waves modeling approach to study the possibilities to detect and, in some instances differentiate, subsurface objects from diffracted or scattered seismic energy. In addition, to the conventional vertical-receivers we used data from horizontal-receivers aligned with the source. Synthetic seismic data sets models suggest that it is possible to observe different seismic responses from voids and boulders. Thus, this method could increase/decrease the likelihood an observed scatter is from a void. In such a manner, these observation can be used to further develop tools for more accurate detection and discrimination of subsurface anomalies.

Introduction

This work is a continuation of a larger research project that was designed to evaluate several seismic techniques to detect, differentiate, identify, and, when possible, estimate the changes in physical characteristics or properties of materials of naturally occurring or human-made near-surface underground structures such as tunnels, mines, voids, etc.

Various seismic methods to detect voids were presented by Sloan et al. (2010) was followed by multi-method approach to detect clandestine tunnels (Sloan et al., 2015). Efforts to detect tunnel using seismic diffractions (Peterie and Miller, 2015; Peterie et al., 2016) extending the works of other researchers (Landa and Keydar, 1998; Grandjean and Leparoux, 2004; Khaidukov et al., 2004) suggested that mode converted diffractions and diffractions related to the shear-wave (S-wave) or surface waves may be generated and in some cases used for imaging (Korneev, 2009; Kaslilar et al., 2013). However, identifying voids from other subsurface objects using the seismic method typically has been a challenging problem (Ivanov et al., 2017).

One of the goals of this research effort was to evaluate the potential of using more than one seismic response events for near surface anomaly detection and possible identification.

Synthetic Seismic Models

Six synthetic seismic data sets were calculated using FFDM, a proprietary software from the Kansas Geological Survey for seismic-data modeling, specifically tuned for the estimation of surface-wave propagation (Zeng et al., 2011). Background seismic model parameters were selected using a 1-layer model (Table 1), which was 450 m wide and 45 m deep.

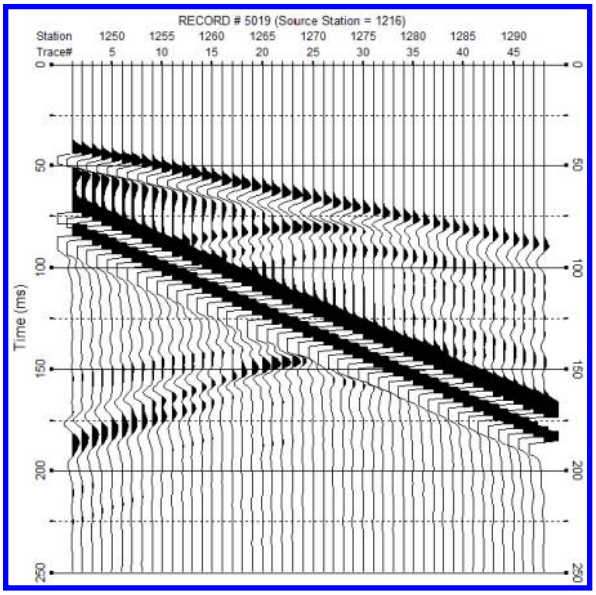

Figure 1. The synthetic seismic shot gather 5019 for an 80 Hz wavelet source stationed at station 1216 (field layout shown on Figure 2) with p-wave diffractions (at ~75 ms) and surface-wave backscatters (at ~145 ms) originating from the void located at station 1270.

One of the models contained a void, another a boulder with velocities two times greater than the background (Table 2), and the third one did not contain any anomalies. Both anomalies were 1.6 x 1.6 m and located at 10 m depth. Forty-eight vertical (V) and 48 longitudinal-oriented horizontal (Sv) receivers were spaced at 1 m, intervals (Figure 1), providing two data sets for each model.

Table 1. The single-layer model parameters used for the calculation of synthetic seismic data.

Layer	V_s(m/s)	V_p(m/s)	Dens. (g/m^3)
1	500	1000	1.8

Table 2. The boulder parameters used for the calculation of synthetic seismic data.

Void	V_s(m/s)	V_p(m/s)	Dens. (g/m^3)
1	1000	2000	2.6

Data were acquired with a roll-along style of survey with source and receivers advancing at 2 m increments. Thirty-two synthetic shot records were calculated from each model using an 80-Hz first derivative Gaussian wavelet located 30 m away from the nearest receiver.

10.1190/segam2018-2998570.1

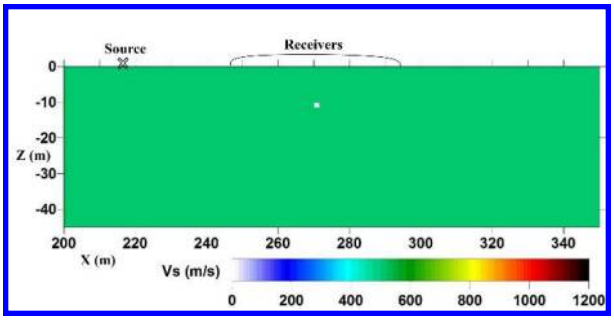

Figure 2. Shear-wave velocity model used for calculating synthetic seismic shot records showing the location of the void (the white square), source (cross), and receivers.

For data processing convenience, the left edge of the void was assigned to the station number 1270 (a horizontal location number) corresponding to x = 270 m (Figure 2). Record 5019 (Figure 1) was calculated using source and receiver locations indicated on the seismic model (Figure 2). The no-anomaly V-receiver data set was subtracted from the corresponding void-containing and boulder containing data sets to obtain clear void-only- and boulder-only-signature data sets. Another pair of void-only- and boulder-only-signature data sets were obtained using the Sv-receivers.

Some of the questions we tried to address included: can we observe both compressional-wave (p-wave) and shear-wave (s-wave) diffraction arrival patterns, how many, would they be different on the void-only and boulder-only signature records, and would there be differences when using V- or Sv-receiver data?

To address these topics we adopted the approach of plotting the diffraction arrival times from the void/boulder following four types of propagation patterns: an incident p-wave and a diffracted p-wave (p-p); an incident p-wave and a diffracted s-wave (p-s); and an incident s-wave and a diffracted p-wave (s-p), and an incident s-wave and a diffracted s-wave (s-s). Additional curves, such as the ones from an incident p-wave, a p-wave multiple from the void to the surface and to the void, and a diffracted s-wave (p-p-s) were plotted when suggested by the arrival patterns.

First we examined the void-only vertical receiver data (Figure 3). It was possible to observe the p-p diffraction arrivals on all traces, the p-s and the p-p-s diffraction arrivals on most of the traces with the exception of 5-7 traces near the apex, and half of the s-p arrivals diffracting back toward the source (i.e., it was difficult to identify s-p diffraction away from the source). Some arrivals matched reasonably well with the s-s body wave diffractions but were in a very close range of a possible Rayleigh wave response, which for this type of model would have a 93.5 % velocity of the shear wave. Observing their lower frequency content and larger amplitudes in comparison to the p-s and the p-p-s arrival, we considered these arrivals to be most likely from the Rayleigh wave. We examined an identical 25-Hz V-receiver void-only synthetic data set (Figure 4) obtained at previous stage of our research efforts (Ivanov et al., 2017).

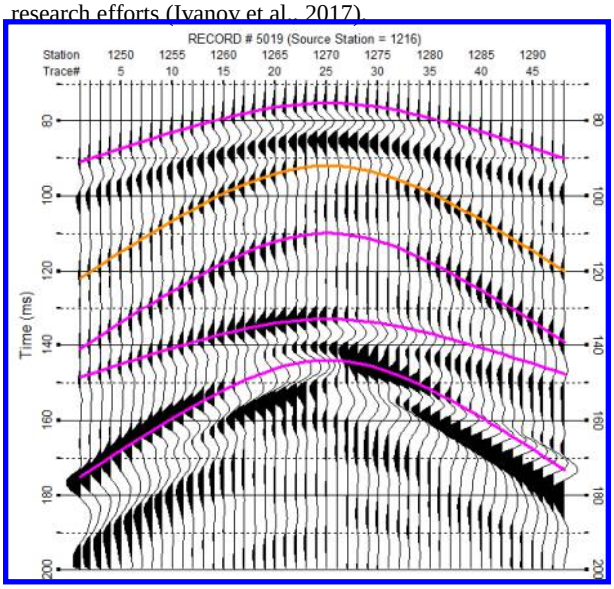

Figure 3. An 80 Hz, void-only V-receiver synthetic seismic shot gather 5019 with a void located at station 1270. Curves from top to bottom follow the diffraction arrival times of the p-p, p-s, p-p-s, s-p, and s-s body waves.

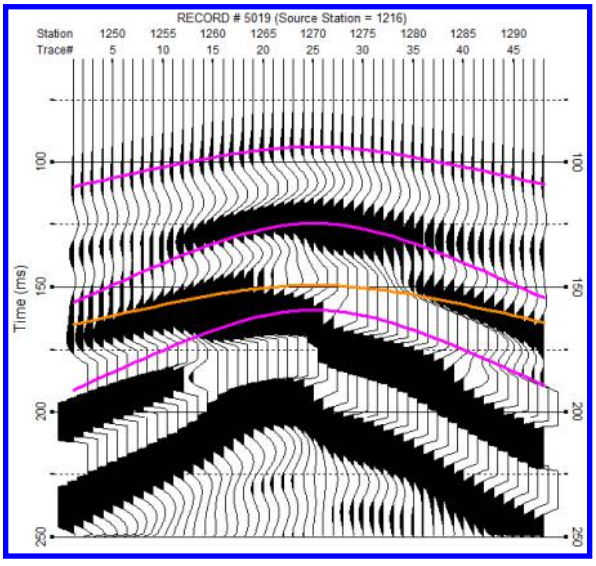

Figure 4. A 25-Hz, void-only V-receiver synthetic seismic shot gather 5019 with a void located at station 1270. Curves from top to bottom follow the diffraction arrival times of the p-p, p-s, s-p, and s-s body waves.

10.1190/segam2018-2998570.1

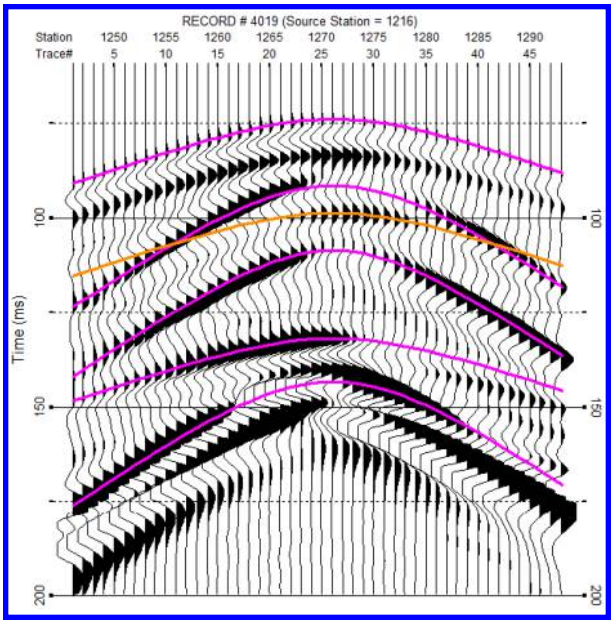

Figure 5. An 80 Hz, boulder-only V-receiver synthetic seismic shot gather 5019 with a void located at station 1270. Curves from top to bottom follow the diffraction arrival times of the p-p, p-s, p-p-p (orange line), p-p-s, s-p, and s-s body waves.

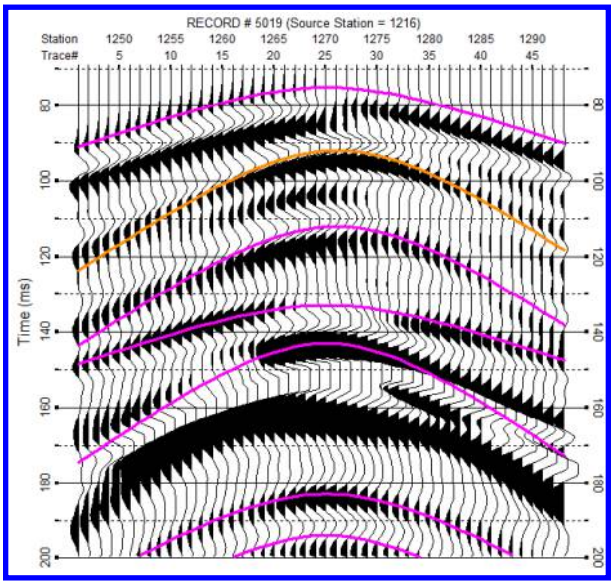

Figure 6. An 80 Hz, void-only Sv-receiver synthetic seismic shot gather 5019 with a void located at station 1270. Curves from top to bottom follow the diffraction arrival times of the p-p, p-s, p-p-s, s-p, s-s body waves, and a pair of possible p-ns-s curves.

As expected, there was significant interference between the lower frequency wavelets and it was difficult to identify any arrival patterns but the ones for the p-p wave. Still, we provide this comparison for continuity and completeness.

Next, we examined the boulder-only vertical receiver data (Figure 5) using positive-polarity fill in the display in comparison to the negative-polarity fill of the void-only data (Figure 3). Similarly, it was possible to observe almost identical diffraction arrivals for the p-p, p-s, p-p-s, s-p, and s-s body waves travel paths. In addition, it was possible to observe ~14 traces matching the diffraction apex of a p-p-p travel path.

Third, we examined the void-only Sv-receiver data (Figure 6). It was possible to clearly observe only the p-p and s-p diffraction arrivals. Their signature was different in comparison to the V-receiver data. The p-p changed polarity at the apex and the s-p was this time was noticeable on most of the traces with the exception of 5-7 traces near the apex, which was similar to the p-s and p-p-s patterns of the V-receiver data.

The p-s and p-p-s arrival curves did not find a good match on void-only Sv-receiver data. The observed potentially s-wave diffractions exhibited apparent velocity ~20-30 % higher than the s-wave velocity of the seismic model (i.e., 500 m/s). Furthermore, it was possible to observe such arrival pairs (with higher gain) ringing ("p-ns-s" curves) down the record below 180 ms (Figure 7). As well, it was possible to observe such an apparent higher velocity for a potential s-s curve (Figure 8).

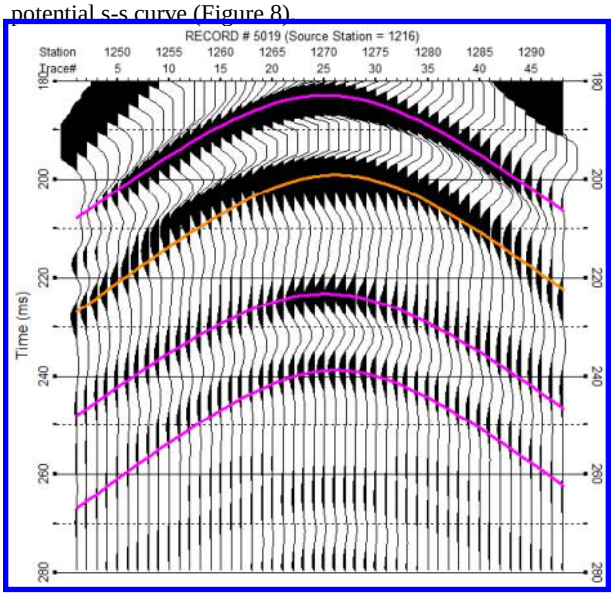

Figure 7. An 80 Hz, void-only Sv-receiver synthetic seismic shot gather 5019 with a void located at station 1270. Curves from top to bottom follow a time-delayed curvatures close to the s-wave diffraction arrival times.

Then, we examined the boulder-only Sv-receiver data (Figure 9). Similarly to the void-only Sv-receiver data, it was

possible to clearly observe only the p-p and s-p diffraction arrivals using a positive-polarity amplitude fill.

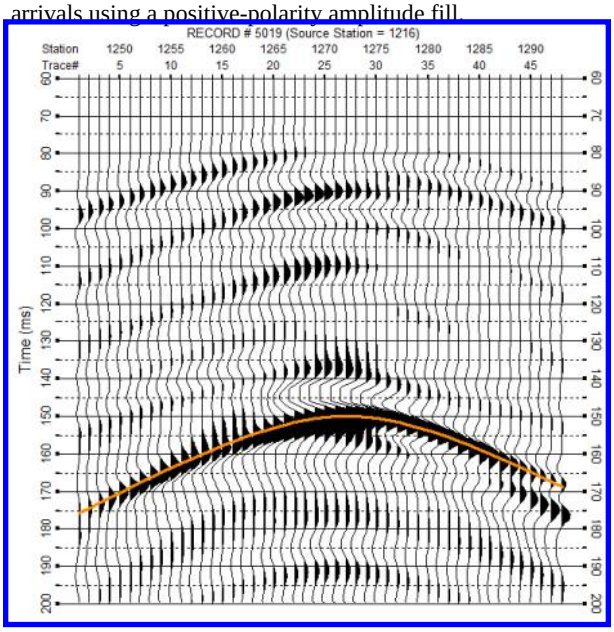

Figure 8. An 80 Hz, void-only Sv-receiver synthetic seismic shot gather 5019 with a lower gain and a void located at station 1270. Curve following potential s-s diffraction arrival times with a 30 % higher apparent s-wave velocity.

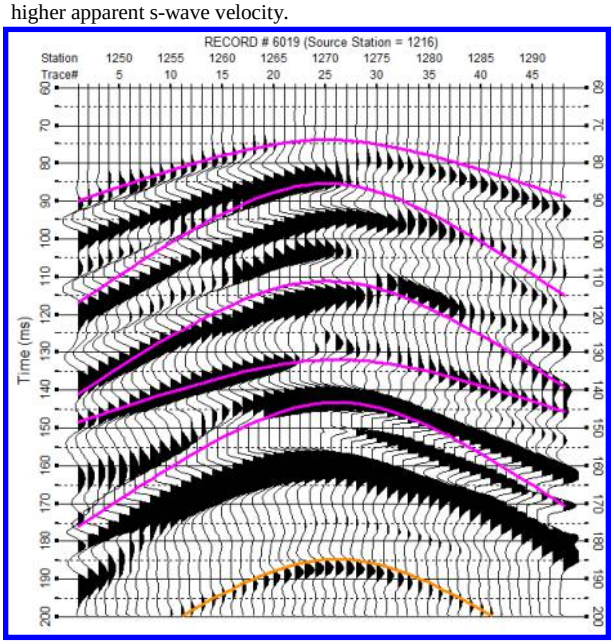

Figure 9. An 80 Hz, boulder-only Sv-receiver synthetic seismic shot gather 5019 with a void located at station 1270. Curves from top to bottom follow the diffraction arrival times of the p-p, p-s, p-p-s, s-p, s-s body waves, and a possible p-ns-s curve.

Likewise, it was possible to observe s ringing ("p-ns-s") patterns below 180 ms with a reduced clarity (Figure 10).

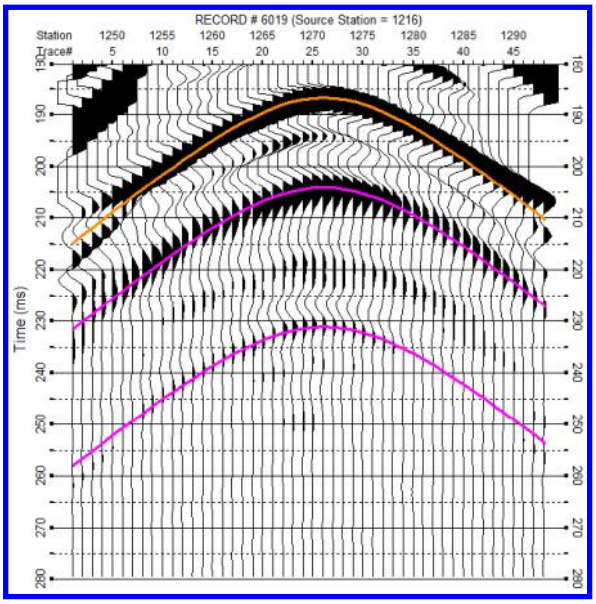

Figure 10. An 80 Hz, boulder-only Sv-receiver synthetic seismic shot gather 5019 with a void located at station 1270. Curves from top to bottom follow a time-delayed curvatures close to the s-wave diffraction arrival times.

For these models, the main difference between the void-only and boulder only V-reciever responses appeared to be the polarity reversal and the presence of a few diffraction-apex p-p-p arrivals. The main difference between the void-only and boulder only Sv-reciever response appears to be the polarity reversal and the ringing patterns below 180 ms.

It was possible to observe clearly only two (p-p and s-p) diffracion patterns with the Sv receivers in comparison to at least four when using V receivers. Further reseach could clarify the 30 % higher apparent diffraction velocity than the model s-wave diffraction arrivals.

Conclusions

Different model- and receiver-data comparisons show that there can be potential for using multiple arrival signatures for enhanced detection and possible identification of near surface underground anomalies using the seismic method.

Acknowledgments

We appreciate Mary Brohammer for her assistance in manuscript preparation.

10.1190/segam2018-2998570.1

REFERENCES

Grandjean, G., and D. Leparoux, 2004, The potential of seismic methods for detecting cavities and buried objects: Experimentation at a test site: Journal of Applied Geophysics, **56**, 93–106, https://doi.org/10.1016/j.jappgeo.2004.04.004.

Ivanov, J., R. D. Miller, D. Z. Feigenbaum, and S. L. Peterie, 2017, Detecting subsurface objects and identifying voids possibilities using the back-scatter analysis of surface wave (BASW) method: International Conference on Engineering Geophysics, 116–119.

Kaslilar, A., U. Harmankaya, K. Wapenaar, and D. Draganov, 2013, Estimating the location of a tunnel using correlation and inversion of Rayleigh wave scattering: Geophysical Research Letters, **40**, 6084–6088, https://doi.org/10.1002/2013GL058462.

Khaidukov, V., E. Landa, and T. J. Moser, 2004, Diffraction imaging by focusing-defocusing: An outlook on seismic superresolution: Geophysics, **69**, 1478–1490, https://doi.org/10.1190/1.1836821.

Korneev, V., 2009, Resonant seismic emission of subsurface objects: Geophysics, **74**, no. 2, T47–T53, https://doi.org/10.1190/1.3068448.

Landa, E., and S. Keydar, 1998, Seismic monitoring of diffraction images for detection of local heterogeneities: Geophysics, **63**, 1093–1100, https://doi.org/10.1190/1.1444387.

Peterie, S., R. Miller, J. Ivanov, Y. Wang, S. Morton, S. Sloan, M. Moran, and H. Cudney, 2016, Tunnel detection using SH-wave diffraction imaging: 86th Annual International Meeting, SEG, Expanded Abstracts, 5006–5010, https://doi.org/10.1190/segam2016-13962354.1.

Peterie, S. L., and R. D. Miller, 2015, Near-surface scattering phenomena and implications for tunnel detection: Interpretation, **3**, no. 1, SF43–SF54, https://doi.org/10.1190/INT-2014-0088.1.

Sloan, S. D., S. L. Peterie, J. Ivanov, R. D. Miller, and J. R. McKenna, 2010, Void detection using near-surface seismic methods, in R. D. Miller, J. D. Bradford, and K. Holliger, eds., Advances in Near-Surface Seismology and Ground-Penetrating Radar: SEG, 201–218.

Sloan, S. D., S. L. Peterie, R. D. Miller, J. Ivanov, J. T. Schwenk, and J. R. McKenna, 2015, Detecting clandestine tunnels using near-surface seismic techniques: Geophysics, **80**, no. 5, EN127–EN135.

Zeng, C., J. H. Xia, R. D. Miller, and G. P. Tsoflias, 2011, Application of the multiaxial perfectly matched layer (M- PML) to near-surface seismic modeling with Rayleigh waves: Geophysics, **76**, no. 3, T43–T52, https://doi.org/10.1190/1.3560019.